Mathematical Modelling and Analysis
Volume 14 Number 1, 2009, pages 43–56
Doi:10.3846/1392-6292.2009.14.43-56

ISSN 1392-6292 print
ISSN 1648-3510 online
www.vgtu.lt/mma/

Numerical Solution of a Model for Brain Cancer Progression after Therapy*

Z. Jackiewicz[1], Y. Kuang[2], C. Thalhauser[3] and B. Zubik-Kowal[4]

[1,2,3]*Arizona State University,* [4]*Boise State University*
[1]Department of Mathematics, Tempe, AZ 85287;
AGH University of Science and Technology, Kraków, Poland
E-mail(*corresp.*): jackiewi@math.la.asu.edu
[2,3]Department of Mathematics, Tempe, AZ 85287
E-mail: kuang@asu.edu; craig@mathpost.asu.edu
[4]Department of Mathematics, Boise, ID 83725
E-mail: zubik@math.boisestate.edu

Received August 8, 2008; published online February 25, 2009

Abstract. We present a numerical scheme used to investigate a mathematical model of tumor growth which incorporates multiple disparate timescales. We simulate the model with different initial data. The initial conditions explored herein correspond to a small remnant of tumor tissue left after surgical resection. Our results indicate that tumor regrowth begins at the pre-surgery tumor-healthy tissue interface and penetrates back into the original tumor area. This growth is rate-limited by the reformation of the tumor vascular network.
Key words: theoretical oncology, mathematical models, numerical methods.

1 Introduction

We propose a mathematical model for tumor growth based upon the assumption that growth and motility are mutually exclusive phenomena [1, 4, 10]. Cells exist in one of two states, and can transit between those states at density dependent per capita rates. We use the Holling type III functional response from the mathematical population theory as the form of these transitions. Growth of tumor cells is limited by a single nutrient, here considered to be oxygen. The model presented here is a simplified variation of the one detailed in [14]. For simplicity, we recreate the heuristic derivation here. More detailed descriptions and justifications of the model and its function forms may be found in

* The work of the first author was partially supported by NSF grant DMS–0509597. The second author was partially supported by NSF grant DMS-0436341 and the grant DMS/NIGMS-0342388 jointly funded by NIH and NSF

[14]. A much more complicated three-dimensional model which is essentially and expanded version of this model is implemented on real brain geometry and validated by a set of clinical data in [5], indicating that the model framework proposed in [14] and used in this paper is robust and plausible.

The two states of this model represent cells locked in a proliferative state and cells locked in a migratory state. Net cellular proliferation is a function of available nutrient, as experimentally quantified in [7, 15]. Migratory cells do not grow, but die at a constant per capita rate. Migration is assumed to be a random walk through the tumor region, with solid boundaries which permit no cells to invade the surrounding healthy tissue.

Based on these assumptions, we give a word model which describes the system and then formalize the model into a set of partial differential equations. The model consists of three dependent variables: migratory cells (M), growing cells (G), and nutrient (O). The word equations for the model are:

$$\begin{aligned}
\text{Change of } M &= \text{Migration} + \text{Transitions from } G \text{ to } M \\
&\quad - \text{Transitions from } M \text{ to } G - \text{Death}, \\
\text{Change of } G &= \text{Birth} - \text{Death} + \text{Transitions from } M \text{ to } G \\
&\quad - \text{Transitions from } G \text{ to } M, \\
\text{Change of } O &= \text{Diffusion} - \text{Consumption}.
\end{aligned}$$

The initial conditions considered in this work correspond to a novel setting for tumor growth. Rather than investigating early tumor development, we assume that such a tumor has already grown, been detected, and removed. Since surgical resection never guarantees removal of all transformed cells [3, 8], we consider initial conditions which dictate different distributions of possible remaining cells and study the nature of tumor regrowth, if in fact it does even regrow. In this setting, we assume spherical symmetry in the region of the excised tumor, and we assume that all vasculature has been removed along with the tumor tissue. Thus, the only source of nutrient to the system is from the exterior boundary.

The organization of this paper is as follows. In Section 2 we provide a mathematical description of the model with new initial conditions corresponding to the distribution of the remaining cancer cells after the therapy. The spatial discretization of the model by pseudospectral method is then described in Section 3. In Section 4 we investigate the equation of the model for the tumor cell density in the proliferation state. In Section 5 we investigate the influence of initial conditions on the stability of computations. The numerical experiments with the model are presented in Section 6. Finally, in Section 7 some concluding remarks are given.

2 Mathematical Model

Let $\rho_M(r,t)$ be the tumor cell density in migratory state, $\rho_G(r,t)$ be the tumor cell density in proliferation state, and $O(r,t)$ be the oxygen concentration. Here, r denotes radius and t denotes time. We consider the following model equations, which are introduced in [14] for the cell densities and the oxygen

concentration:

$$\begin{cases} \dfrac{\partial \rho_M}{\partial t} &= D_\rho \Delta_r \rho_M + \dfrac{\rho^2}{K_M^2+\rho^2}\rho_G - \dfrac{K_G^2}{K_G^2+\rho^2}\rho_M - \mu\rho_M, \\ \dfrac{\partial \rho_G}{\partial t} &= \Phi(O,\rho)\rho_G - \dfrac{\rho^2}{K_M^2+\rho^2}\rho_G + \dfrac{K_G^2}{K_G^2+\rho^2}\rho_M, \\ \dfrac{\partial O}{\partial t} &= D_{0_2}\Delta_r O - \Phi_C(O)\rho_G, \end{cases} \tag{2.1}$$

with the total cell density $\rho(r,t) = \rho_M(r,t)+\rho_G(r,t)$ and the oxygen dependent growth and consumption functions are

$$\begin{aligned} \Phi(O,\rho) &= A\,\frac{O^p}{C_1^p+O^p} - B\left(1-\sigma\frac{O^q}{C_2^q+O^q}\right)\frac{\rho}{\rho_{max}}, \\ \Phi_C(O) &= \gamma\,A\,\frac{O^p}{C_1^p+O^p}. \end{aligned}$$

Here, A and B are the maximal oxygen dependent growth and death rates, respectively. Constants C_1 and C_2 are the oxygen thresholds and p and q are the cooperativity coefficients for their respective processes. The constant σ is considered to be a survival scaling factor, although its biological interpretation is vague. The constant γ is a conversion factor relating oxygen concentration to the cell density. The Laplacian $\Delta_r\rho_M$ is given by

$$\Delta_r\rho_M = \frac{\partial^2\rho_M}{\partial r^2} + \frac{2}{r}\frac{\partial\rho_M}{\partial r}$$

with $\Delta_r\rho_G$ defined in a similar way. The system (2.1) has to be supplemented with the initial and boundary conditions. As in [14] we will always assume that the boundary conditions take the form

$$\begin{cases} \dfrac{\partial\rho_M(0,t)}{\partial r} = \dfrac{\partial\rho_M(R,t)}{\partial r} = 0, \\ \dfrac{\partial O(0,t)}{\partial r} = 0, \quad O(R,t) = C_0, \end{cases} \tag{2.2}$$

where $C_0 > 0$ is a given constant. We consider a modification of the initial conditions considered in [14] which correspond to a specific tumor development. These conditions are given by

$$\rho_M(r,0) = 0, \quad r\in[0,R], \tag{2.3}$$

$$\rho_G(r,0) = \begin{cases} 8.3912\cdot 10^{-6}\cdot\exp\left(-\dfrac{r^2}{0.005}\right), & 0\le r<0.2, \\ 0, & 0.2\le r\le R, \end{cases} \tag{2.4}$$

$$O(r,0) = 95, \quad r\in[0,R]. \tag{2.5}$$

As already mentioned in Section 1 in this paper we also consider a novel setting and assume that the tumor has already grown, has been detected and removed.

This corresponds to different initial conditions which dictate different distributions of the remaining cells, and we assume that

$$\rho_M(r,0) = 10^{-6}, \quad r \in [0,R], \tag{2.6}$$

$$\rho_G(r,0) = 8.3912 \cdot 10^{-6} \cdot \exp\Big(-\frac{r^2}{0.005}\Big), \quad r \in [0,R], \tag{2.7}$$

where $O(r,0)$ is defined as in [14] by (2.5). Notice that the initial functions (2.5), (2.6) and (2.7) are even with respect to r and can be symmetrically extended over the interval $[-R,R]$. The overall new model consisting of (2.1), boundary conditions (2.2), and the initial conditions (2.5), (2.6) and (2.7) will be discretized with respect to the space variable r by pseudospectral method and then integrated in time by the code `ode15s` from Matlab ODE suite [12].

3 Pseudo-spectral Radial Discretization

To compute numerical approximations to the unknown functions ρ_M, ρ_G, O we discretize the system (2.1) with respect to $r \in [-R,R]$ by pseudo - spectral method based on the Chebyshev-Gauss-Lobatto points $r_i = -R\cos\big(\frac{i\pi}{N}\big)$, for $i = 0,1,\ldots,N$. To omit the point of singularity $r = 0$ we apply only odd numbers N. We have chosen this method because it is fast, efficient, and very accurate. Pseudo-spectral methods are exponentially convergent, i.e., the error behaves like $O(\alpha^N)$ for some $0 < \alpha < 1$, compare [6, 9], while the finite difference methods converge only with polynomial rate, i.e., the error behaves like $O(1/N^p)$ for some integer p, the order of the method. Hence, we can employ a significantly smaller number of grid points N to get a comparable accuracy to finite difference methods with a much larger number of grid points.

The first order derivatives $\partial\rho_M(r_i,t)/\partial r$ can be replaced by the spectrally accurate approximations

$$\frac{\partial\rho_M(r_i,t)}{\partial r} \approx \sum_{j=0}^{N} d_{i,j}^{(1)}\rho_M(r_j,t) \tag{3.1}$$

for $i = 0,1,\ldots,N$. Here, $D^{(1)} = \big[d_{i,j}^{(1)}\big]_{i,j=0}^{N}$ is the differentiation matrix of the first order, compare [2] and [11]. The approximations (3.1) and the boundary conditions (2.2) lead to

$$d_{0,0}^{(1)}\rho_M(r_0,t) + \sum_{j=1}^{N-1} d_{0,j}^{(1)}\rho_M(r_j,t) + d_{0,N}^{(1)}\rho_M(r_N,t) \approx 0,$$

$$d_{N,0}^{(1)}\rho_M(r_0,t) + \sum_{j=1}^{N-1} d_{N,j}^{(1)}\rho_M(r_j,t) + d_{N,N}^{(1)}\rho_M(r_N,t) \approx 0,$$

which results in the approximations for $\rho_M(r_0,t)$ and $\rho_M(r_N,t)$ of the form

$$\rho_M(r_0,t) \approx \rho_0(t) = \frac{d_{0N}^{(1)} \sum_{j=1}^{N-1} d_{N,j}^{(1)} \rho_M(r_j,t) - d_{NN}^{(1)} \sum_{j=1}^{N-1} d_{0,j}^{(1)} \rho_M(r_j,t)}{d_{00}^{(1)} d_{NN}^{(1)} - d_{0N}^{(1)} d_{N0}^{(1)}}, \quad (3.2)$$

$$\rho_M(r_N,t) \approx \rho_N(t) = \frac{d_{N0}^{(1)} \sum_{j=1}^{N-1} d_{0,j}^{(1)} \rho_M(r_j,t) - d_{00}^{(1)} \sum_{j=1}^{N-1} d_{N,j}^{(1)} \rho_M(r_j,t)}{d_{00}^{(1)} d_{NN}^{(1)} - d_{0N}^{(1)} d_{N0}^{(1)}}.$$

Let us define

$$D = \begin{bmatrix} d_{11}^{(1)} & \dots & d_{1,N-1}^{(1)} \\ \vdots & \ddots & \vdots \\ d_{N-1,1}^{(1)} & \dots & d_{N-1,N-1}^{(1)} \end{bmatrix}, \quad d_0 = \begin{bmatrix} d_{10}^{(1)} \\ \vdots \\ d_{N-1,0}^{(1)} \end{bmatrix}, \quad d_N = \begin{bmatrix} d_{1N}^{(1)} \\ \vdots \\ d_{N-1,N}^{(1)} \end{bmatrix},$$

$$\rho_M(t) = \begin{bmatrix} \rho_M(r_1,t) \\ \vdots \\ \rho_M(r_{N-1},t) \end{bmatrix}, \quad \big(\rho_M\big)_r(t) = \begin{bmatrix} \dfrac{\partial \rho_M(r_1,t)}{\partial r} \\ \vdots \\ \dfrac{\partial \rho_M(r_{N-1},t)}{\partial r} \end{bmatrix},$$

$$\big(\rho_M\big)_{rr}(t) = \begin{bmatrix} \dfrac{\partial^2 \rho_M(r_1,t)}{\partial r^2} \\ \vdots \\ \dfrac{\partial^2 \rho_M(r_{N-1},t)}{\partial r^2} \end{bmatrix}, \quad I_r = \begin{bmatrix} \dfrac{1}{r_1} \\ \vdots \\ \dfrac{1}{r_{N-1}} \end{bmatrix}.$$

Then, the approximations (3.1) and (3.2) lead to

$$\big(\rho_M\big)_r(t) \approx D\,\rho_M(t) + \rho_0(t)\,d_0 + \rho_N(t)\,d_N. \quad (3.3)$$

Now, applying (3.3) with (2.2) gives

$$\big(\rho_M\big)_{rr}(t) \approx D^2\,\rho_M(t) + \rho_0(t)\,D\,d_0 + \rho_N(t)\,D\,d_N. \quad (3.4)$$

The approximations (3.3) and (3.4) result in

$$\begin{aligned} \Delta_r \rho_M \approx{}& D^2\,\rho_M(t) + \rho_0(t)\,D\,d_0 + \rho_N(t)\,D\,d_N \\ &+ 2I_r \cdot \big(D\,\rho_M(t) + \rho_0(t)\,d_0 + \rho_N(t)\,d_N\big), \end{aligned} \quad (3.5)$$

where '$\cdot$' stands for component-wise multiplication of vectors.

It can be checked that the denominators in (3.2) satisfy the inequalities

$$\left| d_{00}^{(1)} d_{NN}^{(1)} - d_{0N}^{(1)} d_{N0}^{(1)} \right| > 120, \quad \text{for all} \quad N \geq 8.$$

Therefore, computing the approximations $\rho_0(t)$ and $\rho_N(t)$ from (3.2) does not cause significant rounding errors. However, since the boundary conditions in (2.2) are different for the functions ρ_M and O, for the Laplacian $\Delta_r O$, we apply a different approximation than (3.5). For this approximation, we take the advantage from the fact that the values of O are known at the boundaries and are given exactly by C_0 (the boundary condition for O in (2.2)). To derive the approximation for $\Delta_r O$ we apply (3.1) with ρ_M replaced by O and additionally we apply the spectrally accurate approximation

$$\frac{\partial^2 O(r_i,t)}{\partial r^2} \approx \sum_{j=0}^{N} d_{i,j}^{(2)} O(r_j,t), \quad i=0,1,\ldots,N,$$

where $D^{(2)} = \left[d_{i,j}^{(2)}\right]_{i,j=0}^{N}$ is the differentiation matrix of the second order, compare with [2, 11]. Let the vectors $O(t)$, $(O)_r(t)$ and $(O)_{rr}(t)$ be defined in the same way as the vectors $\rho_M(t)$, $(\rho_M)_r(t)$ and $(\rho_M)_{rr}(t)$. Then the vector $(O)_r(t)$ is approximated by

$$(O)_r(t) \approx D\,O(t) + C_0\,d_0 + C_0\,d_N \tag{3.6}$$

and the vector $(O)_{rr}(t)$ is approximated by

$$(O)_{rr}(t) \approx D_2\,O(t) + C_0\,d_0^{(2)} + C_0\,d_N^{(2)}. \tag{3.7}$$

Here,

$$D_2 = \begin{bmatrix} d_{11}^{(2)} & \cdots & d_{1,N-1}^{(2)} \\ \vdots & \ddots & \vdots \\ d_{N-1,1}^{(2)} & \cdots & d_{N-1,N-1}^{(2)} \end{bmatrix}, \quad d_0^{(2)} = \begin{bmatrix} d_{10}^{(2)} \\ \vdots \\ d_{N-1,0}^{(2)} \end{bmatrix}, \quad d_0^{(2)} = \begin{bmatrix} d_{10}^{(2)} \\ \vdots \\ d_{N-1,0}^{(2)} \end{bmatrix}.$$

From (3.6) and (3.7) we obtain the approximation

$$\Delta_r O \approx D_2\,O(t) + C_0\,d_0^{(2)} + C_0\,d_N^{(2)} + 2I_r \cdot \big(D\,O(t) + C_0\,d_0 + C_0\,d_N\big). \tag{3.8}$$

Application of (3.5) and (3.8) to (2.1) results in the semi-discrete system

$$\begin{cases} \dfrac{d\rho_M(t)}{dt} = D_\rho\,D^2\,\rho_M(t) + \rho_0(t)\,D\,d_0 + \rho_N(t)\,D\,d_N, \\ \qquad\qquad +2I_r \cdot \big(D\,\rho_M(t) + \rho_0(t)\,d_0 + \rho_N(t)\,d_N\big) + f^{(1)}(t), \\ \dfrac{d\rho_G(t)}{dt} = f^{(2)}(t), \\ \dfrac{dO(t)}{dt} = D_{0_2}\,D_2\,O(t) + C_0\,d_0^{(2)} + C_0\,d_N^{(2)}, \\ \qquad\qquad +2I_r \cdot \big(D\,O(t) + C_0\,d_0 + C_0\,d_N\big) + f^{(3)}(t), \end{cases} \tag{3.9}$$

with the vectors $f^{(i)}(t) = \left(f_1^{(i)}(t), \ldots, f_{N-1}^{(i)}(t)\right)^T$, $i = 1, 2, 3$, defined by

$$f_j^{(1)}(t) = \frac{\rho^2(r_j,t)}{K_M^2 + \rho^2(r_j,t)}\rho_G(r_j,t) - \frac{K_G^2}{K_G^2 + \rho^2(r_j,t)}\rho_M(r_j,t) - \mu\rho_M(r_j,t),$$

$$f_j^{(2)}(t) = \Phi(O(r_j,t), \rho(r_j,t))\rho_G(r_j,t) - \frac{\rho^2(r_j,t)}{K_M^2 + \rho^2(r_j,t)}\rho_G(r_j,t),$$

$$f_j^{(3)}(t) = -\Phi_C(O(r_j,t))\rho_G(r_j,t), \quad j = 1, 2, \ldots, N-1.$$

The resulting semi-discrete system (3.9) of differential equations is stiff and in the next sections, we apply the code `ode15s` from the Matlab ODE suite [12] to compute approximations to ρ_M, ρ_G, and O. This code is designed for stiff differential systems. It is much more efficient than the code `ode45` based on embedded pair of explicit Runge-Kutta methods of order $p = 4$ and $p = 5$ which is designed for non-stiff equations.

4 Investigations of the Equation for the Tumor Cell Density in the Proliferation State

In this section, we investigate the second equation of the model (2.1). It is used to compute the tumor cell density $\rho_G(r,t)$ in the proliferation state and it can be written in the form:

$$\frac{\partial\rho_G}{\partial t} = \lambda(r,t)\rho_G + \frac{K_G^2}{K_G^2 + \rho^2}\rho_M, \tag{4.1}$$

with the variable coefficient

$$\lambda(r,t) = \Big(A\,\frac{O^p}{C_1^p + O^p} - B\left(1 - \sigma\frac{O^q}{C_2^q + O^q}\right)\frac{\rho}{\rho_{max}} - \frac{\rho^2}{K_M^2 + \rho^2}\Big). \tag{4.2}$$

Since the functions $O(r,t)$ and $\rho(r,t) = \rho_M(r,t) + \rho_G(r,t)$ are symmetric about the $r = 0$ axis, $\lambda(r,t)$ has the same property. Our goal is to investigate the sign of the function $\lambda(r,t)$ for $t \geq 0$ and $r \in [0,R]$.

Note that $\lambda(r,t)$ evolves differently for different initial functions $\rho(r,0)$ and $O(r,0)$. Fig. 1 shows different coefficients $\lambda(r,t)$ computed by the definition (4.2) with the functions $\rho(r,t)$ and $O(r,t)$ obtained from model (2.1)-(2.2) supplemented by three different sets of initial conditions:

1. (2.3), (2.4), and (2.5) for case (a),
2. (2.5), (2.6), and (2.7) for case (b),
3. (2.5), (2.7) and
$$\rho_M(r,0) = 10^{-7}, \quad r \in [0,R], \tag{4.3}$$
for case (c).

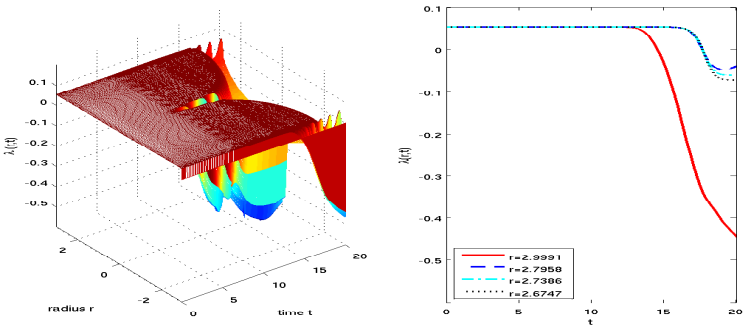

Case (a): $\lambda(r,t)$ with numerical solutions started from (2.3)-(2.5)

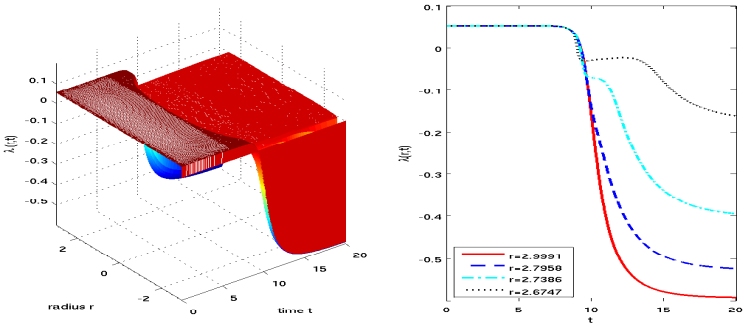

Case (b): $\lambda(r,t)$ with numerical solutions started from (2.5)-(2.7)

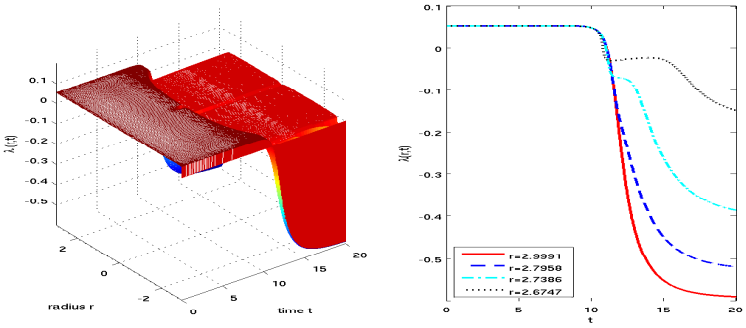

Case (c): $\lambda(r,t)$ with numerical solutions started from (2.5), (2.7), and (4.3)

Figure 1. The coefficient $\lambda(r,t)$ for three different cases $a) - c)$.

Case (a) corresponds to early tumor development without medical treatment, compare with [14], where the modification of this condition is considered; while cases (b) and (c) correspond to tumor development after surgical resection of already grown tumors which may remain transformed cells, [3], [8].

For Fig. 1, the numerical approximations to $\rho_M(r,t)$, $\rho_G(r,t)$, and $O(r,t)$ are computed by solving the semi-discrete system (3.9) for $r \in [-R,R]$. We apply the code `ode15s` (see [12]) with $AbsTol = 10^{-8}$ and $RelTol = 10^{-6}$ to integrate (3.9) in time and then we use the definition (4.2) to compute the approximations to $\lambda(r,t)$. To compute the numerical approximations to $\rho_M(r,t)$, $\rho_G(r,t)$, and $O(r,t)$, for $r \in [-R,R]$, we extend the corresponding initial conditions over the interval $[-R,R]$ by using the fact that the all three initial functions in the cases (a), (b), and (c) are even as functions of r.

Note that, since $A > 0$, by the definition (4.2), the initial functions in cases (a),(b) and (c) imply

$$\lambda(r,0) > 0, \quad \text{for all } \ r \in [-R,R].$$

Since $\lambda(r,t)$ is a continuous function, this inequality is maintained also for $t > 0$ which are close to zero. This observation is confirmed by the numerical experiments presented in Fig. 1. However, Fig. 1 shows that the values of the function $\lambda(r,t)$ start to be negative for $t > T$, with some T sufficiently large. Moreover, $\lambda(r,t) < 0$, for $t > T$ and even all $r \in [-R,R]$, in the cases (b) and (c). This shows that the numerical computations for the model (2.1)-(2.2) are stable provided that stable numerical methods are applied to the semi-discrete system (3.9) to integrate it in time t.

The goal of this paper is to investigate the cases (b) and (c), which correspond to the cancer development from the cells remained after surgical resections of previously grown tumors. The case (a) was investigated in [14]. In Section 5, we present results of numerical experiments for the cases (b) and (c). The experiments show stable computations and confirm the above analysis of the coefficient $\lambda(r,t)$.

5 Analysis of Initial Conditions for the Cancer Model in Spherical Coordinates

The goal of this section is to investigate the numerical solutions to $\rho_G(r,t)$ and $\rho_M(r,t)$ started at $t = 0$ from different initial functions, which correspond to different surgical resections. We consider three different sets of initial conditions which correspond to a small remnants of tumor cells after surgery. These conditions are given by:

1. (2.5), (2.6) and (2.7) for case (b),
2. (2.5), (2.7) and (4.3) for case (c),
3. (2.5), (2.7) and $\rho_M(r,0) = 10^{-6}\left(\exp\left(-\frac{(r^2-1)^2}{0.5}\right)+1\right)$ for case (d).

We would like to mention again that the case (a) in Section 4 corresponds to early tumor development. Some modification of this condition was investigated in [14].

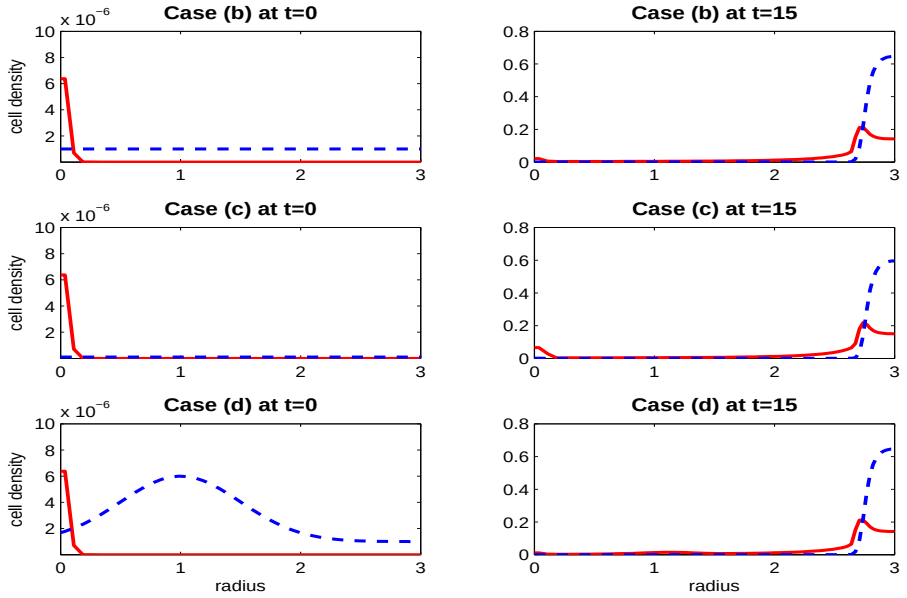

Figure 2. Numerical solutions to (2.1)–(2.2) at $t = 15$ days (right-hand side pictures) and their initial values at $t = 0$ (left-hand side pictures). Proliferating cells are denoted by solid lines and migrating cells by dashed lines.

Note that all of the initial functions are even with respect to r and can be symmetrically extended over the interval $[-R, R]$. The initial functions are presented in the first column of Fig. 2. In the cases (b) and (c), the tumor cell density in proliferation state is distributed uniformly for $r \in [0, R]$, while in the case (d), the density is nonuniform with a maximum located at $r = 1$. In the case (d), the originally grown tumor was not uniformly removed during the surgical resection which left transformed cells distributed in a nonuniform way (Fig 2, case (d) at $t = 0$). The leftover cells initiate further developments of new tumors. The densities of the new regrown cells are presented in the second column of Fig 2.

The second column of Fig 2 shows numerical approximations to $\rho_G(r, t)$ and $\rho_M(r, t)$ at $t = 15$ days. In all of the cases (b), (c) and (d) the tumor densities regrow. Although the initial conditions are different in the case (d) than in the cases (b) and (c), the regrowths develop similarly in all of the cases. Moreover, Fig 2 shows that the regrown cells are concentrated at the boundary of the surgical resection site.

Fig. 3 presents numerical approximations to $\rho_G(r, t)$ and $\rho_M(r, t)$ at $t = 5, 10, 15$ in the cases (b) and (c). We observe that both densities $\rho_G(r, t)$ and $\rho_M(r, t)$ are somewhat higher in case (b) than in case (c). This can be explained

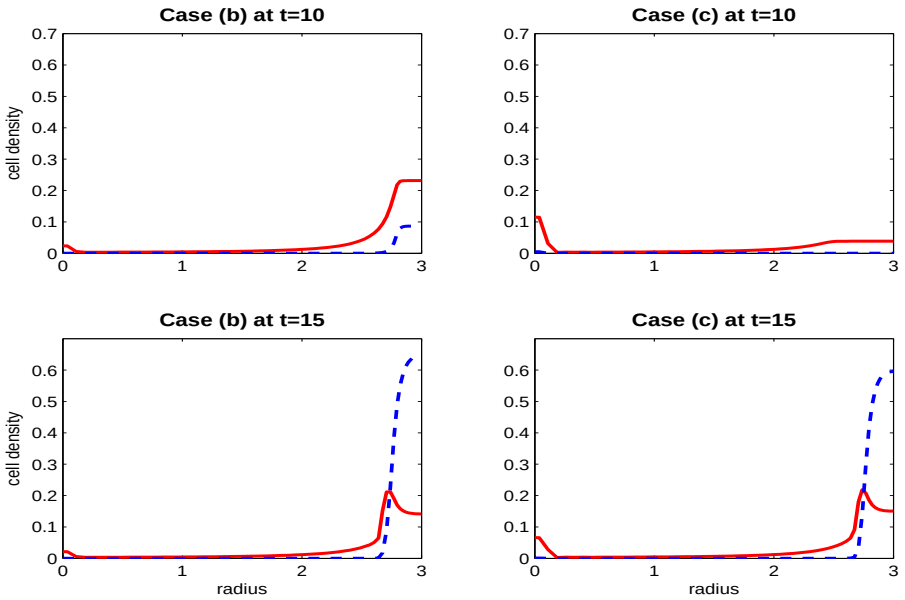

Figure 3. The numerical solutions to (2.1)–(2.2), (2.5) and (2.7) with ρ_M started from the initial function (2.6): left-hand side pictures, and from (4.3): right-hand side pictures. Proliferating cells are denoted by solid lines and migrating cells by dashed lines.

by the fact that the initial function $\rho_M(r,0)$ is 10 times larger in case (b) than in case (c).

The numerical solutions from Fig. 2 and 3 are obtained by the pseudospectral radial discretization on the interval $[-R,R]$ and by the code `ode15s`. The parameter $N=128$ is used for the pseudospectral method and $AbsTol=10^{-8}$, $RelTol=10^{-6}$ are applied for the time integration. Because of symmetry of the solutions, they are presented only on the part $[0,R]$.

6 Numerical Computations of Tumor Cell Densities and Oxygen Concentrations

In this section, we investigate the model (2.1)–(2.2) supplemented by the initial conditions (2.5)–(2.7).

Fig. 4 presents tumor cell densities in migratory and proliferation states after $t=8$, 9, 10, 11, 12, 14, 35, and 40 days. The pictures of Fig. 4 show differences between the cell densities developed in different time ranges. We observe that the cells grow rapidly between $t=5$ and $t=14$ days, their growth slows down between $t=14$ and $t=35$ and after $t=35$ days the cell densities do not change. Therefore, we conclude that, for (2.5)–(2.7), the most significant changes in the tumor development occur between the 8th and the 14th day.

The development of the oxygen concentration is presented in Fig. 5. After about $t=12$ days the oxygen concentration stays constant like in Fig. 4, where

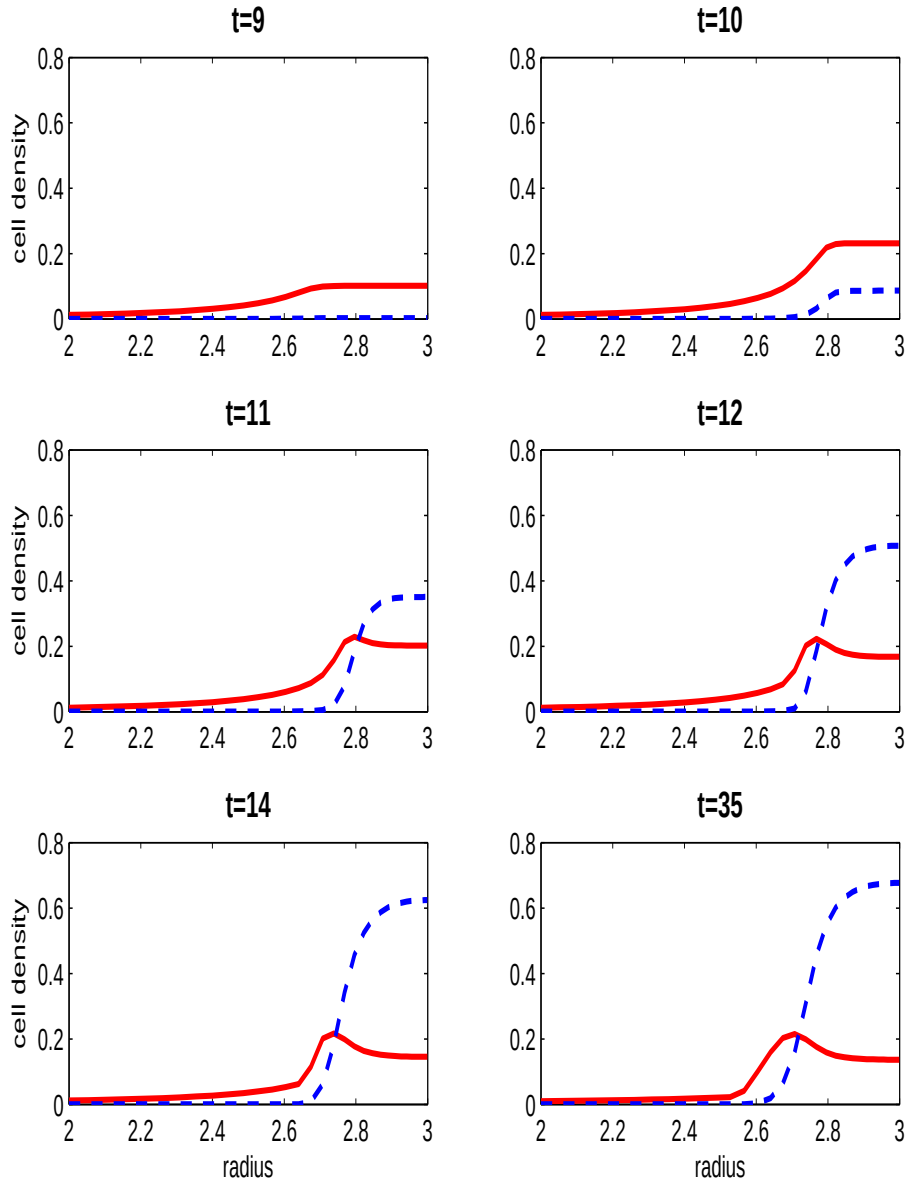

Figure 4. The numerical solutions $\rho_M(r,t)$ and $\rho_G(r,t)$ to (2.1)–(2.2), (2.5)–(2.7). Proliferating cells are denoted by solid lines and migrating cells by dashed lines.

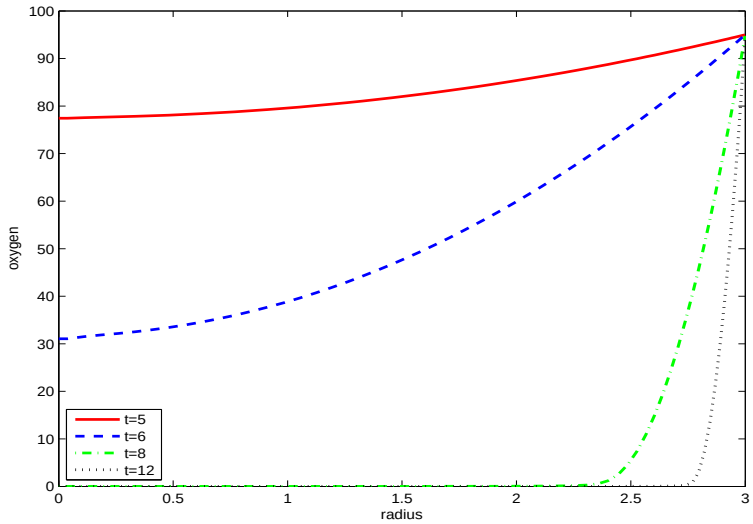

Figure 5. The numerical solution $O(r,t)$ to (2.1)–(2.2), (2.5)–(2.7). After 12 days the oxygen values $O(r,t)$ stay the same.

the tumor cell densities stay constant after about $t = 35$. Moreover, Fig. 4 and 5 show that the tumor cell densities, especially in migratory state (dotted lines), are higher in the regions with higher oxygen concentration and lower in the regions with lower oxygen concentration.

7 Conclusions

As shown in Fig. 3 and 4, we observe a quick ($t < 14$ days) regrowth of tumor density back into the vacant cavity. This regrowth is driven primarily by leftover migratory cells converting back into a proliferative state in a suddenly nutrient-rich environment. This regrowth occurs at the boundary of the surgical resection site; cells more towards the core have little opportunity to establish a large colony (compare initial condition densities 1 and 2 in Section 5 with resulting steady state densities in Figures 4 and 5). The inward extent of growth is limited by consumption of diffusible nutrients (Fig. 5). Taken together, the data generated by this model suggest that the process of tumor recurrence after surgery is rate-limited by the reconstruction of the angiogenic network needed to support large tumor structures. Given the timescale disparities between clinically observed bulk tumor growths (order weeks to months, see [13] for example) versus small-scale tumor growth (order days), one could approximate the rate of vascularization by the rate of bulk tumor expansion.

Acknowledgments

The authors wish to express their gratitude to anonymous referees for their useful comments.

References

[1] A.J. Bolteus, M.E. Berens and G.J. Pilkinton. Migration and invasion in brain neoplasms. *Current Neurology and Neuroscience Reports*, **1**:225–232, 2001.

[2] Canuto C., Hussaini M.Y., Quarteroni A. and Zang T.A. *Spectral Methods in Fluid Mechanics*. Springer Verlag, New York, 1988.

[3] M.C. Chamberlain. Treatment options for glioblasma. *Neurosurgical Focus (electronic)*, **20**(4, E2), 2006.

[4] T. Demuth and M.E. Berens. Molecular mechanisms of glioma cell migration and invasion. *Journal of Neuro-Oncology*, **70**:217–228, 2004.

[5] S. Eikenberry, T. Sankar, M.C. Preul, E.J. Kostelich, C. Thalhauser and Y. Kuang. The virtual glioblastoma: growth, migration, and treatment in three-dimensional mathematical model. *Cell Proliferation*. (to appear)

[6] B. Fornberg. *A Practical Guide to Pseudospectral Methods*. Cambridge University Press, Cambridge, New York, 1996.

[7] D. Gammack, H.M. Byrne and C.E. Lewis. Estimating the selective advantage of mutant $p53$ tumour cells to repeated rounds of hypoxia. *Bull. Math. Biol.*, **63**:135–166, 2001.

[8] A. Giese, R. Bjerkvig, M.E. Berens and M. Westphal. Cost of migration: invasion of malignant gliomas and implications for treatment. *Journal of Clinical Oncology*, **21**:1624–1636, 2003.

[9] J.S. Hesthaven, S. Gottlieb and D. Gottlieb. *Spectral Methods for Time-Dependent Problems*. Cambridge University Press, Cambridge, New York, 2007.

[10] D.B. Hoelzinger, J. Mariani, L.and Weis, T. Woyke, T.J. Berens, W.S. McDonough, A. Sloan, S.W. Coons and M.E. Berens. Gene expression profile of glioblastoma multiforme invasive phenotype points to new therapeutic targets. *Neopasia*, **7**:7–16, 2005.

[11] Trefethen L.N. *Spectral Methods in Matlab*. SIAM,Philadelphia, 2000.

[12] L.F. Shampine and M.W. Reichelt. The Matlab ODE suite. *SIAM J. Sci. Comput.*, **18**:1–22, 1997.

[13] K.R. Swanson, Alvord Jr. E.C. and J.D. Murray. A quantitative model for diffrential motility of gliomas in grey and white matter. *Cell Proliferation*, **33**:317–329, 2000.

[14] C.J. Thalhauser, T. Sankar, M.C. Preul and Y. Kuang. Explicit separation of growth and motility in a new tumor cord model. *Bull. Math. Biol.* (to appear)

[15] K.E. Thompson and J.A. Royds. Hypoxia and reoxygenation: A pressure for mutant $p53$ cell selection and tumour progression. *Bull. Math. Biol.*, **61**:759–778, 1999.